International Soil and Water Conservation Research 10 (2022) 586–596

Contents lists available at ScienceDirect

International Soil and Water Conservation Research

journal homepage: www.elsevier.com/locate/iswcr

Original Research Article

Field instrumentation for real-time measurement of soil-water characteristic curve

Abdul Halim Hamdany [a], Yuanjie Shen [a], Alfrendo Satyanaga [b], Harianto Rahardjo [c, *], Tsen-Tieng Daryl Lee [d], Xuefeng Nong [a]

[a] School of Civil and Environmental Engineering, Nanyang Technological University, Block N1, #B1a-01a, 50 Nanyang Avenue, Singapore, 639798
[b] Department of Civil and Environmental Engineering, Nazarbayev University, Nur-Sultan, 010000, Kazakhstan
[c] School of Civil and Environmental Engineering, Nanyang Technological University, Block N1, #1B-36, 50 Nanyang Avenue, Singapore, 639798
[d] CUGE Research, National Parks Board Singapore, 1 Cluny Rd, Singapore, 259569

ARTICLE INFO

Article history:
Received 28 November 2020
Received in revised form
26 January 2022
Accepted 28 January 2022
Available online 11 February 2022

Keywords:
Suction measurement
Tensiometer
Moisture sensor
SWCC
Field measurement

ABSTRACT

Suction measurement has a vital role in unsaturated soil analysis. However, measuring soil suction remains a challenging task due to a number of issues such as the limited range of suction measurement, cavitation, or long equilibrium time. It is even more challenging when the suction measurement is to be carried on the field. Hence, the development of a new suction measurement device which is able to measure high suction range for a long duration without tedious maintenance and yet portable enough for site measurement is required. In this study, a new sensor which is referred to as NTU Osmotic Tensiometer was developed along with the method to correct for decay and temperature. The NTU osmotic tensiometer is based on polymer swelling capacity in order to measure in-situ soil suction in real time for a very long duration. It requires minimum maintenance as the polymer-based sensor is not affected by the cavitation phenomenon. However, correction for decay and temperature is of paramount importance and therefore explained in this paper. Verification of the NTU osmotic tensiometer was carried out by comparing the field measurement results from the NTU osmotic tensiometer and the small tip tensiometer. The performance of the NTU osmotic tensiometer was found to be comparable with that of the small tip tensiometer, but the NTU osmotic tensiometer is able to measure more than 100 kPa soil suction. Therefore, it is possible to obtain the field soil-water characteristic curve by combining the measured in-situ soil suction from the NTU osmotic tensiometer with the measured in-situ water content from the moisture sensor as illustrated in the paper.

1. Introduction

In Singapore, the deep groundwater table in residual soil slopes creates an unsaturated soil zone above the water table (Rahardjo and Satyanaga, 2019). Although saturated soil slopes are simple to model, many residual soil slopes are commonly unsaturated (Rahardjo et al., 2007). The incorporation of unsaturated soil mechanics may therefore be more representative of actual slope conditions. In unsaturated soil mechanics, the soil's engineering behavior is influenced by the soil's suction and soil-water characteristic curve (SWCC) (Kristo et al., 2017). Seepage through the unsaturated soil is governed by its permeability function and suction changes, which in turn cause changes in its shear strength (Rahardjo, Kim, & Satyanaga, 2019).

A vadose zone extends from the ground surface to the groundwater table. It is also referred to as the unsaturated zone as the water content is lower compared to the saturated zone below it (Fredlund & Rahardjo, 1993). Soil suction, or negative pore-water pressure, in the vadose zone is affected by flux boundary conditions such as evapotranspiration. In vegetated soils, root uptake of water can be significant, depending on the distribution of roots and processes of evapotranspiration. Therefore, pore-water pressures

* Corresponding author.
E-mail addresses: ahhamdany@ntu.edu.sg (A.H. Hamdany), jimmy.shen@ntu.edu.sg (Y. Shen), alfrendo.satyanaga@nu.edu.kz (A. Satyanaga), chrahardjo@ntu.edu.sg (H. Rahardjo), daryl_lee@nparks.gov.sg (T.-T.D. Lee), jasonnong@ntu.edu.sg (X. Nong).

https://doi.org/10.1016/j.iswcr.2022.01.007

are consistently lower or soil suctions are higher in vegetated areas as compared to non-vegetated areas (Satyanaga & Rahardjo, 2019, 2020). Variations in soil suction with water content are represented through SWCCs. Water content can be expressed in terms of volumetric water content, degree of saturation, and gravimetric water content, but the SWCC is generally defined as the changes in volumetric water content with respect to changes in soil suction (Satyanaga et al., 2017).

The conventional way to measure SWCC is using the pressure plate method. However, this process can be expensive, labour-intensive, and time-consuming. Most SWCC tests in the laboratory are conducted without the application of confining pressure which may result in the inaccuracy of SWCC data (Satyanaga et al., 2019; Rahardjo, Satyanaga, et al., 2019). In addition, cyclic wetting-drying has an important influence on the SWCC (Kristo et al., 2019; Zhai et al., 2017a,b, 2018). Hence, it is important to have actual measurements of SWCC in the field. In addition, the climatic condition will affect the actual SWCC data as indicated by the scanning curve of SWCC.

Soils in the field are subjected to an extreme drying and wetting cycle due to weather changes (evapotranspiration and infiltration). Thus, instruments which can be used to measure negative pore-water pressure and volumetric water contents are very important tools for understanding and monitoring the changes in pore-water pressures and moisture contents due to the changes in weather conditions. There are two commonly used methods in measuring soil suction (Ridley and Burland, 1993): the direct measurement method using tensiometer or pressure plate and the indirect measurement method using psychrometer, filter paper, or gypsum (thermal block). However, measurement of negative pore-water pressure remains a challenging task due to several limitations such as:

(1) Direct measurement is commonly limited to −60 to −101 kPa (depends on the purity of water) due to the cavitation phenomenon (Guan & Fredlund, 1997; Ridley and Burland, 1993) while soil suction on site especially near the ground surface can be very high due to evaporation and transpiration from vegetation.
(2) A long equilibrium time for indirect measurement (Ridley and Burland, 1993; Satyanaga et al., 2017) may cause the instrument to be unable to respond to rapid changes induced by changes in flux boundary conditions which occur on-site.

In order to overcome the limited range of soil suction and long equilibrium time, high-capacity tensiometers which are able to measure negative pore-water pressure as low as −1500 kPa was developed by a number of researcher (Lourenço et al., 2006). The practicality of high-capacity tensiometer has been shown to be versatile for laboratory measurements and has been integrated into many unsaturated soil tests. Chen et al. (2015) developed an integrated high capacity tensiometer for continuous measurement of SWCC of a compacted kaolin with high accuracy. Liu et al. (2020) used high capacity tensiometers for measurement of drying and wetting SWCC of low plasticity clay soil. Lourenço et al. (2011) proposed an appropriate procedure for measurement of drying and wetting SWCCs based on discrete and continuous approaches. Toll et al. (2013) developed an automated suction control system for measurement of drying and wetting SWCCs using high suction tensiometers. Wijaya and Leong (2016) utilized high capacity tensiometers in constant water content oedometer test. Wijaya et al. (2014) measured pore-water pressures during constant rate strain, compression tests using high capacity tensiometers. Unfortunately, a high-capacity tensiometer requires re-saturation with a high pressure whenever it cavitates when reaching its maximum capacity or when it is subjected to a cycle of drying and wetting for a long period Wijaya and Leong (2016). Toll et al. (2012) managed to apply a high capacity tensiometer for field measurements. However, a special arrangement is required to ensure that the high capacity tensiometer can be removed easily from the field in order to be re-saturated.

This study aims to evaluate the performance of the new suction probe and water content sensors for the measurement of the real-time soil-water characteristic curve of residual soil during drying and wetting periods in Singapore. The scope of work includes the characterization of unsaturated properties of the residual soil from Jurong Formation in NTU, suction and water content measurements as well as climatic data monitoring within a slope in NTU. The real-time soil-water characteristic curves from field measurements are verified with the drying and wetting soil-water characteristic curve envelope from experimental works in the laboratory.

2. Methodology

2.1. Soil-water characteristic curve and hysteresis model

Properties of unsaturated soil such as permeability, shear strength, and volume change are highly affected by soil suction or negative pore-water pressure and its water content (Zhai et al., 2017a; Fredlund & Rahardjo, 1993; Fredlund et al., 2012). The analysis of unsaturated soil is based on SWCC which describes the relationship between water content (which can be represented by either gravimetric water content, w, volumetric water content, θ, and degree of saturation, S) and soil suction (Fredlund & Xing, 1994; Leong & Rahardjo, 1997; Satyanaga et al., 2013; Wijaya et al., 2015).

It is important to note that SWCC will experience hysteresis when the soil is subjected to drying and wetting due to irregularities in the cross-sections of the void passages or the “ink-bottle” effects (Haines, 1930; Zhai et al., 2018), the contact angle being greater in an advancing meniscus than in a receding meniscus, different amounts of entrapped air during drying and wetting, thixotropic regain or aging due to the wetting and drying history of the soil. The hysteresis in SWCC is as illustrated by Pham et al. (2005) in Fig. 1.

Fig. 1 shows that besides the main drying and wetting of soil, the soil also follows the scanning curves in between the drying and wetting curves. Several hysteresis models have been proposed and evaluated by Pham et al. (2005); Zhai et al. (2020a, 2019, 2017b). Zhai, Rahardjo, Satyanaga, Dai, and Du (2020) also developed an advanced mathematical equation to estimate the hysteresis of SWCC. However, the developed model is only applicable for sandy soils. One of the common hysteresis models used by many researchers to estimate hysteresis for the fine- and coarse-grained soils was developed by Feng and Fredlund (1999) and it has been simplified by Pham et al. (2005). Feng and Fredlund (1999) proposed the following equation to represent the drying SWCC:

$$\theta = \frac{\theta_{u,d} b_d + c_d . s^{d_d}}{b_d + s^{d_d}} \quad (1)$$

where $\theta_{u,d}$ is the maximum water content at drying curve, b_d, c_d, and d_d are the empirical parameters for the Feng and Fredlund (1999) drying SWCC equation. An identical equation can be used to represent the wetting SWCC:

$$\theta = \frac{\theta_{u,w} b_w + c_w . s^{d_w}}{b_w + s^{d_w}} \quad (2)$$

where $\theta_{u,w}$ is the maximum water content at the wetting curve, b_w,

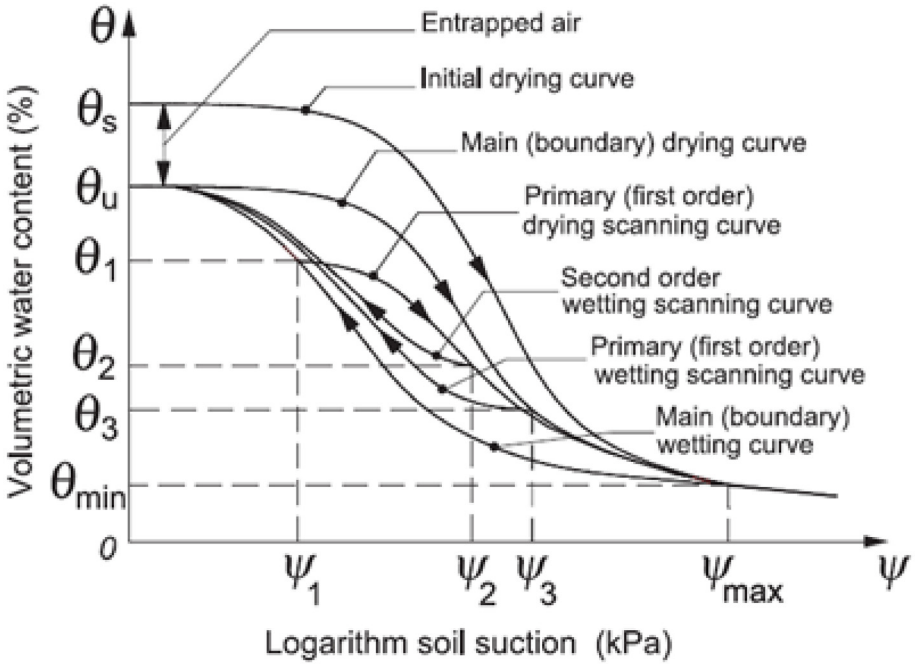

Fig. 1. Hysteresis in SWCC (Pham et al., 2005).

c_w, and d_w are the empirical parameters for the Feng and Fredlund (1999) wetting SWCC equation.

Pham et al. (2005) suggested a simple scaling model to easily obtain Feng and Fredlund (1999) wetting SWCC parameters as follows:

$$b_w = \left[\frac{b_d}{\left(10^{D_{SL}}\right)^{d_d}}\right]^{\frac{1}{R_{SL}}} \quad (3)$$

$$d_w = \frac{d_d}{R_{SL}} \quad (4)$$

$$c_w = c_d \quad (5)$$

where D_{SL} and R_{SL} are the distance and slope ratio between the two boundary curves on the semilogarithmic suction scale. The values of D_{SL} and R_{SL} are different for different soil types as studied by Pham et al. (2005). Pham et al. (2005) suggested to incorporate Fredlund and Xing (1994) correction factor which is represented as follows:

$$C(s) = 1 - \frac{\ln\left(1 + \frac{s}{s_r}\right)}{\ln\left(1 + \frac{10^6}{s_r}\right)} \quad (6)$$

where C(s) is the Fredlund and Xing (1994) correction factor which can be incorporated with Feng and Fredlund (1999) drying and wetting SWCC equation in order to ensure the SWCC will reach 0 at soil suction of 10^6 kPa and S_r is the residual soil suction. For the wetting curve, $\theta_{u,w}$ can be determined from the maximum volumetric water content at the wetting curve or to be estimated as 0.9 θ_s (Pham et al., 2005).

2.2. Slope model subjected to cycle of drying and wetting

Most landslides usually occur during infiltration (Sun et al., 2016) as matric suction decreases during the wetting process. However, it is important to note that slope is also subjected to evaporation and evapotranspiration process. Hence, both drying and wetting processes occur due to climatic conditions (Sweeney, 1982). Tami et al. (2004) conducted a slope model experiment that verified the hysteresis behavior due to the cycle of drying and wetting. Typical experimental data from drying and wetting SWCC are presented in Fig. 2. Air entry value (AEV) as the suction value where air starts to enter the soil is also indicated in Fig. 2. When the slope model was subjected to a drying and wetting cycle, the volumetric water content and the matric suction data points followed the scanning curve prior to reaching the drying curve, and then followed the scanning curve prior to reaching the wetting curve. Thus, for field measurements that have been subjected to a cycle of drying and wetting, it is expected that the data points are located along the scanning curves.

2.3. Calibrations of instruments

NTU developed polymeric osmotic tensiometer (NTU Osmotic Tensiometer consist of piezoresistive pressure transmitter (PAA35x, KELLER) and modified housing cap with 3 bar ceramic disc as shown in Fig. 3. The osmotic tensiometer utilizes the cross-linked polymer as adsorbent materials in place of water for the measurement of negative pore-water pressure (Peck & Rabbidge, 1969; Bocking & Fredlund, 1979; Biesheuvel & Verweij, 1999; Bakker et al., 2007). Superabsorbent polymer (0.1 g of sodium polyacrylate) was used as the filling polymer material to generate high and stable swelling pressure. Table 1 lists the properties of the sodium polyacrylate used in this study. Its large particle size avoids this cross-linked polymer from escaping through the ceramic disc. The high cross-linked density ensures improved consistency of measurement output (Rahardjo et al., 2020).

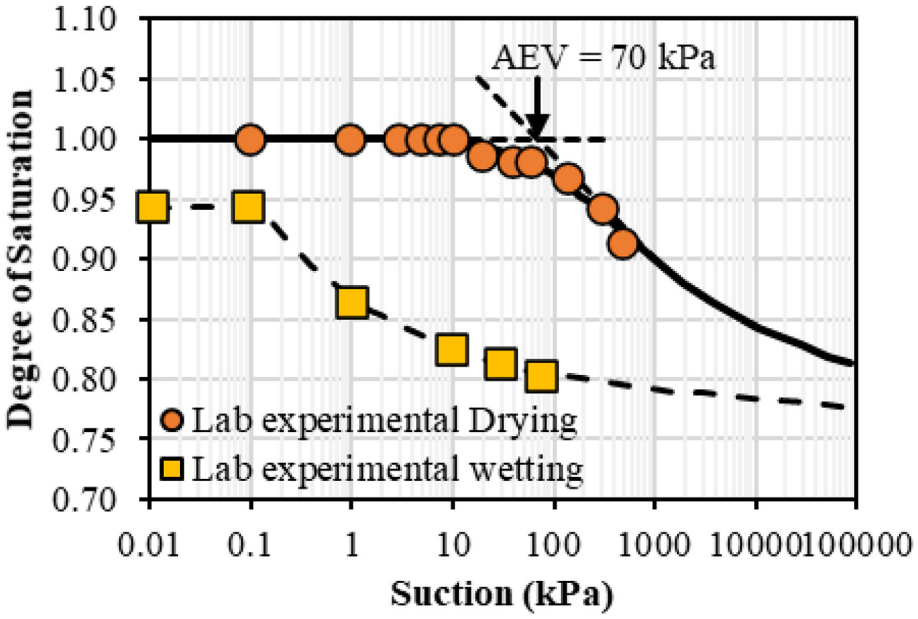

Fig. 2. Typical drying and wetting soil-water characteristic curves.

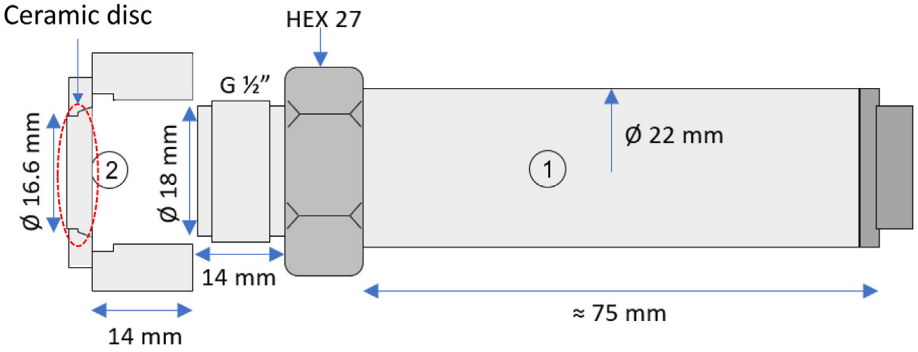

Fig. 3. Schematic drawing of NTU Osmotic Tensiometer (1) PAA-35X Keller Transmitter and (2) New design of cap.

The polymer-based tensiometer is pre-saturated to reach theoretical osmotic pressure based on the osmotic potential of the polymer-water solution (Bakker et al., 2007). The new design for the load cap is meant to reduce the decay rate significantly from the previous design in Rahardjo et al., 2020. The sensor has a pressure range from 0 to 30 bar with an IP68 rating for weather protection. Laboratory calibration was carried out prior to instrumentation installation for temperature and decay correction.

After the polymer is placed inside the NTU Osmotic Tensiometer, the NTU Osmotic Tensiometer is then submerged inside the submersible water chamber which is filled with distilled water as shown in Fig. 4. The osmotic pressure will increase until maximum osmotic pressure is achieved (approximately within 1–2 h) and is recorded by the transducer. The maximum osmotic pressure is then used as the reference point for zero suction. The NTU Osmotic Tensiometer is left inside the submersible water chamber for a week for temperature and decay calibration.

Table 1
Properties of sodium polyacrylate.

Property	Value
Chemical Formula	$C_5H_7NaO_3$
Molecular Weight	94.04 g/mol
Particle Size	90–850 μm
Crosslinking	Cross-linked
Density	0.54 g/mL at 25 °C

2.4. Field instrumentations

Field instrumentation was carried out to demonstrate the performance of NTU Osmotic Tensiometer. A field site was set up in the slope behind the School of Civil and Environmental Engineering, Nanyang Technological University. The coordinates of the field site are 1.345891, 103.678673. The criteria adopted for the site selection was based on two basic conditions: i) places with relevant elevation changes (≥3 m) and ii) locations close to NTU to facilitate for ease of installation and maintenance.

NTU Osmotic Tensiometer (2 unit), moisture sensor (1 unit), and a set of total weather station were installed at the CEE Slope, NTU. Fig. 5 shows the slope geometry and instrumentation of sensors at CEE Slope. The NTU Osmotic Tensiometer and moisture sensor were pushed into the desired locations at 0.5m depth using a driven tool to ensure firm contacts with in-situ soils. Another NTU Osmotic Tensiometer were also installed near the ground surface at 0.15m depth to investigate the effect of root zone on the measurement of

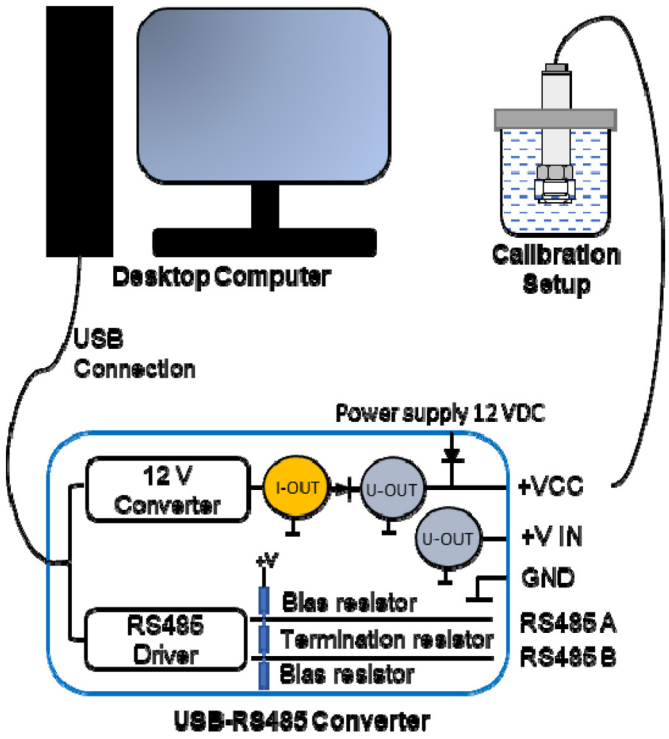

Fig. 4. Setup for calibration of NTU Osmotic Tensiometer in the lab by using submersible water chamber.

soil suction. Polyvinyl chloride pipes with 4" diameter were placed around the sensors to protect them from outside environment. The pipe was extended to the depth of sensor and protruded 0.5m above the ground surface for surface protection.

The moisture sensor measures the soil volumetric moisture content using the standing wave principles. This sensor is used in conjunction with the developed NTU osmotic tensiometer. The moisture sensor is powered by a Lithium-Ion battery with a built-in solar charging controller connected to a solar panel. These sensors provide real-time soil volumetric water content monitoring. The data are transmitted through cable connection using the data logger installed in the enclosure box. The wireless communication enables data transfer up to 250 m in the distance and the data logger is manageable with a supported instrument software. Fig. 6 presents the soil moisture connection in the field that can be monitored remotely from office using wireless communication.

The newly developed NTU Osmotic Tensiometer are installed in the field after completion of the laboratory calibrations. The sensors were installed at different depths (0.15m and 0.5m) which are connected by cable to the junction box and a data logger. Real-time field measurements from the osmotic tensiometers are transmitted using cellular wireless networks. The enclosure box provide housing for an autonomous data logger and a remote data transmission device. The logger can be configured for a specific data collection resolution. The transmitted monitoring measurements are received, processed, stored and presented by the open source software with a time interval of 10 min per data point. The data storage capacity is sufficient enough to last at least an entire year depending on the measurement frequency. The autonomous data logger dan remote transmission device is battery-powered instruments with expected battery life is approximately two years. Data transmission system is shown in Fig. 7.

A total weather station collects information on climatic data with a group of different housed sensors. The real-time monitoring

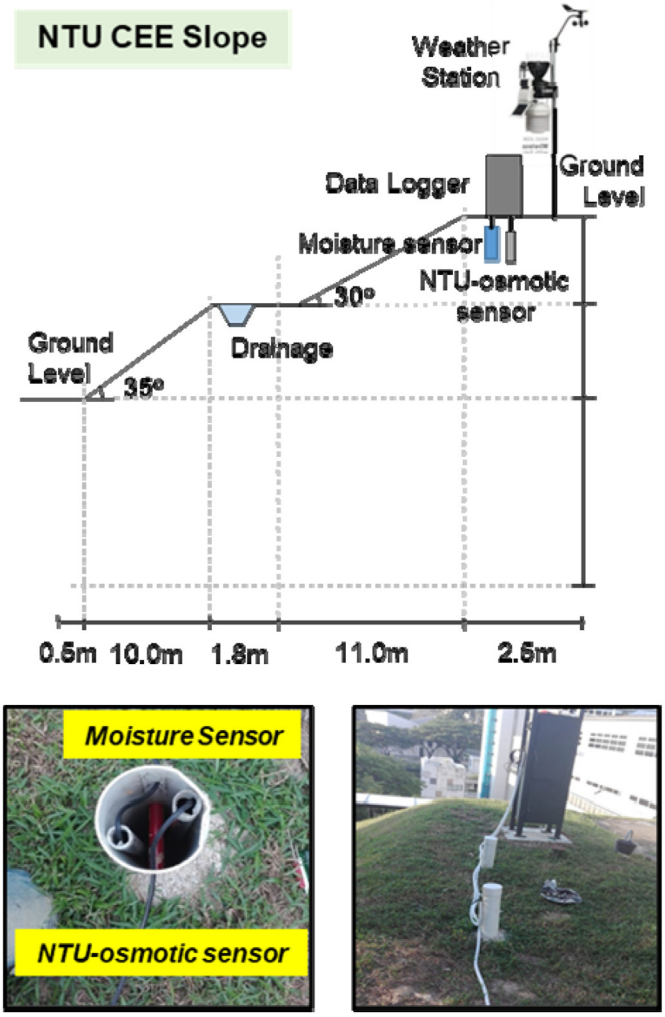

Fig. 5. Geometry of CEE slope and instrumentation of sensors.

from the weather station includes recordings of temperature, rainfall, and humidity. This weather station is powered by a solar panel and set to transmit data to the cloud storage server using a cellular wireless connection. Weather data was uploaded into a commercial weather service provider for real-time weather information. The result can be observed remotely in a public weather server, www.wunderground.com.

3. Results and discussion

3.1. Calibration of NTU osmotic tensiometer

Fig. 8 shows the typical NTU Osmotic Tensiometer uncorrected readings. NTU Osmotic Tensiometer is affected by two phenomena which are cyclic temperature effect and pressure decay. For site measurements, where long test duration is expected (expected for 1-year measurement), two calibrations which are referred to as temperature correction and decay correction are required. Decay correction is required due to cross link between polymer becomes weaken over time. Hence, without decay correction, the suction measured will be much higher compared to the actual suction on site. The temperature correction is important to remove noise on the suction measurement due to the temperature on site. The effect of temperature as shown in Fig. 8 could go up to 40 kPa for 7° change in temperature.

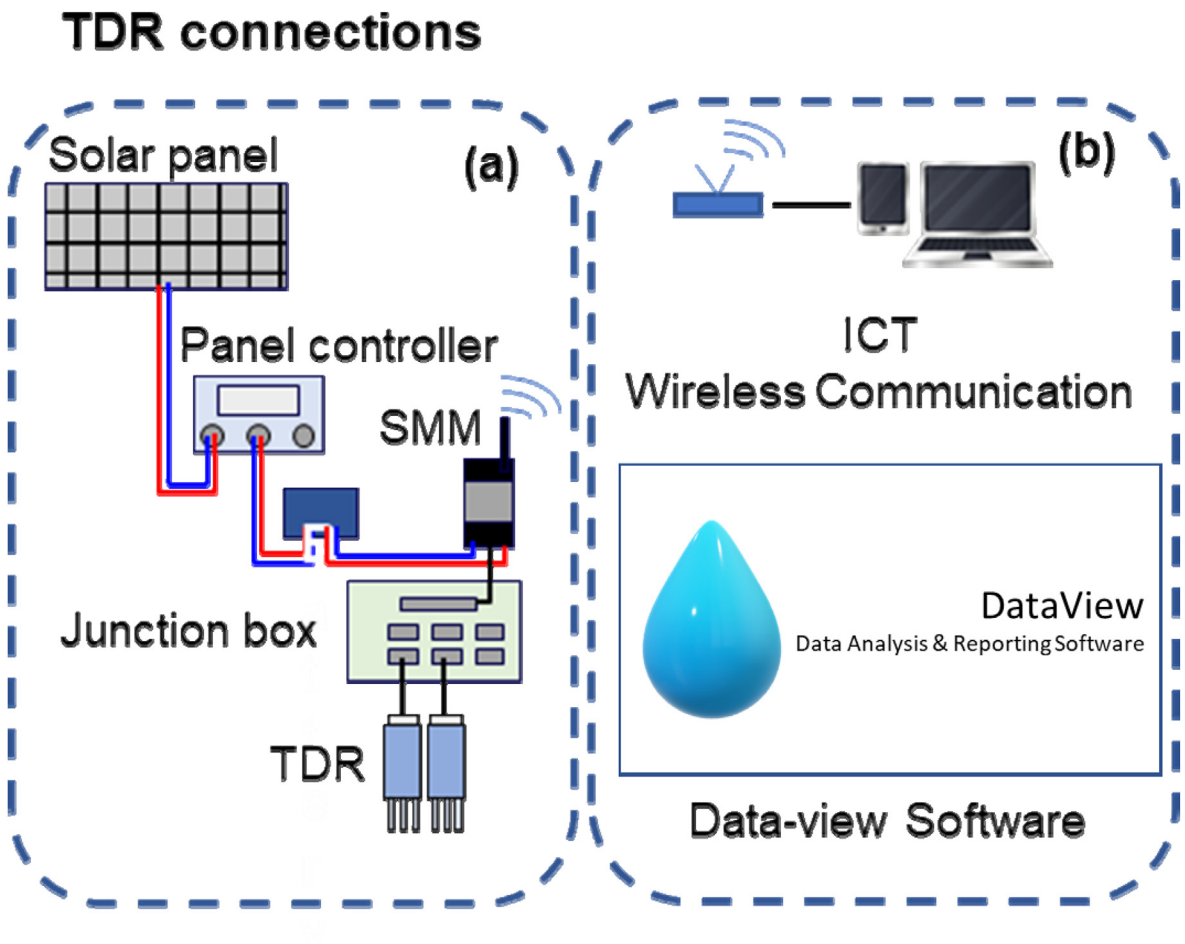

Fig. 6. (a) Moisture sensor system and (b) real-time monitoring interface.

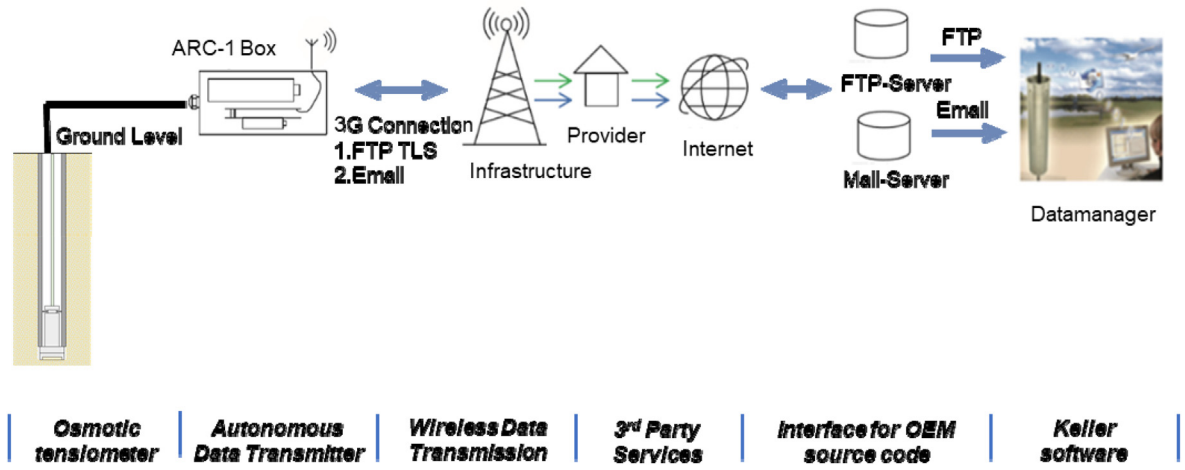

Fig. 7. Data transmission system.

The calibration procedure was carried out in the laboratory under a controlled environment. The NTU Osmotic Tensiometer was submerged under water in a submersible chamber (zero pressure) for a long period in order to obtain the reading which is shown in Fig. 8. Temperature correction can be done by plotting the suction and temperature measurements as shown in Fig. 9. The linear regression shown in Fig. 9 can be represented as follows:

$$\Delta s_T = m_T t + c_T \quad (7)$$

where Δs_T is the suction correction due to temperature, m_T and c_T are the suction correction parameters. Based on Fig. 9, m_T is −9.23 and c_T is 283.14. The measured suction after being corrected for temperature (S_T) is given as:

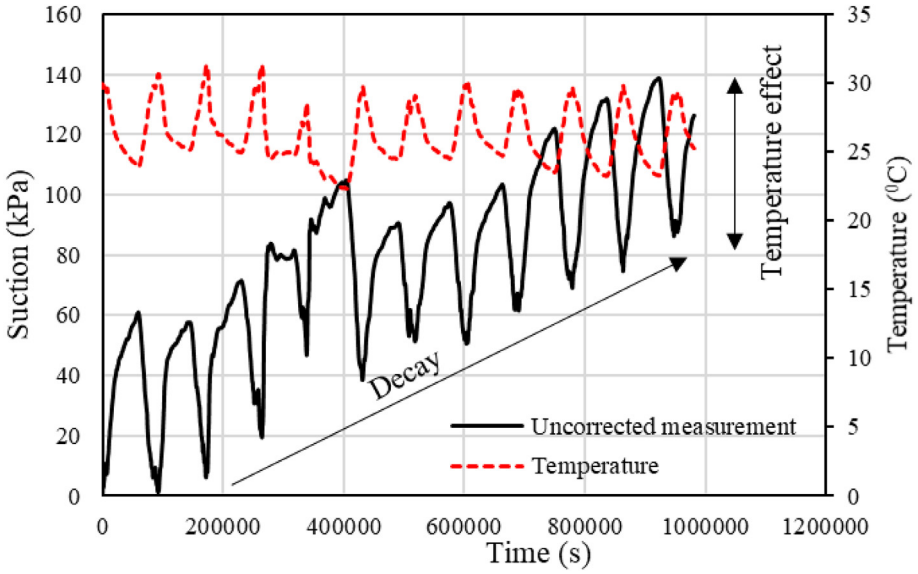

Fig. 8. Typical NTU Osmotic Tensiometer uncorrected reading.

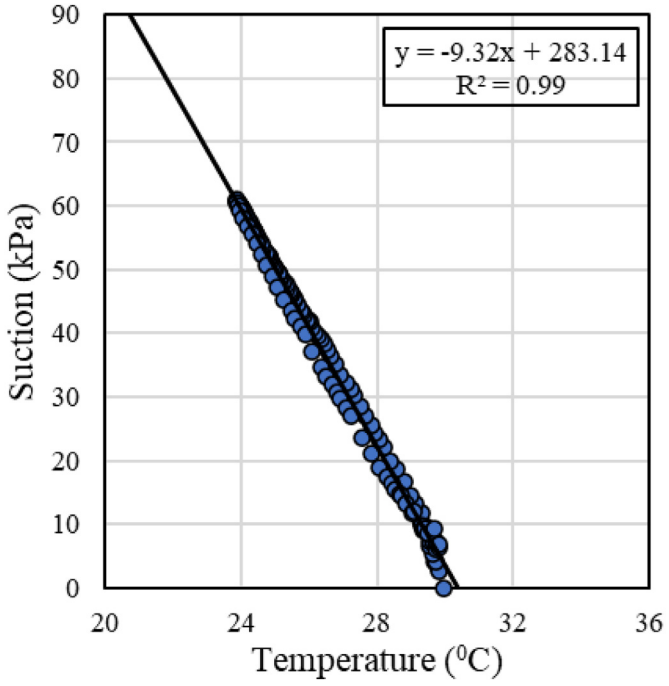

Fig. 9. Calibration for temperature correction.

$$s_t = s_{uncor} - \Delta s_T \quad (8)$$

where s_{uncor} is the uncorrected measured suction.

Fig. 10 shows that the temperature correction works very well and the decay increases linearly over time. In order to correct for the decay, the following equation is proposed:

$$\Delta s_d = m_d(t_i - t_0) \quad (9)$$

where Δs_d is the correction for decay, m_d is the regression parameter, t_i is the current time, while t_0 is the time when the suction probe fully saturated. The corrected suction (s) can then be obtained as follow:

$$s = s_t - \Delta s_d \quad (10)$$

Fig. 10 shows that a corrected suction is about zero all the time as the NTU Osmotic Tensiometer is saturated inside the submersible chamber.

3.2. Field suction monitoring

Two NTU Osmotic Tensiometers were installed at depth 0.15 m (root zone) and 0.50 m (below root zone). A moisture sensor probe was installed at depth 0.50 m as well. Fig. 11 shows the field suction monitoring for NTU Osmotic Tensiometer located at 0.15m depth, plotted together with temperature and its uncorrected suction. The corrected suction is the measured suction that has been corrected for decay and temperature. It is shown that the calibration is very important to be carried out as temperature keeps changing on site and decay also occurs.

Fig. 12 shows the corrected readings from the two NTU Osmotic Tensiometers together with the accumulated rain fall per week from the total weather station. Based on Fig. 12, it shows that NTU Osmotic Tensiometer responds well with the changes in flux boundary conditions (i.e., rainfall and evapotranspiration). When the rain fall intensity is high, the measured soil suction is low especially after rain. On the other hand, when the rain fall intensity is low, the soil suction starts to build up. NTU Osmotic Tensiometer located at the root zone shows an erratic fluctuation because the shallow surface zone is more sensitive to the evapotranspiration while NTU Osmotic Tensiometer located below the root zone shows that the soil suction increases gradually and it is not as affected by the evapotranspiration as much as the NTU Osmotic Tensiometer located at the root zone.

Small tip tensiometer was installed at 0.5m depth in order to compare its measurement with the NTU Osmotic Tensiometer which was installed at the same depth of 0.5m. The small tip tensiometer and the NTU Osmotic Tensiometer were located 3m apart from each other. Fig. 13 shows the comparison between NTU Osmotic Tensiometer and small tip tensiometer measurements.

Fig. 13 shows that both NTU Osmotic Tensiometer and small tip tensiometer measurements had a similar trend and magnitude,

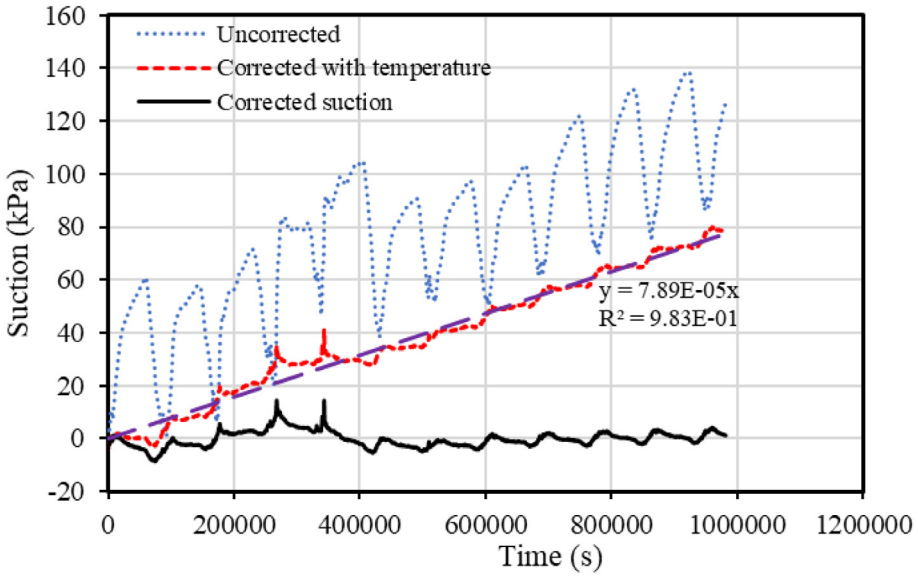

Fig. 10. Calibration for decayed correction.

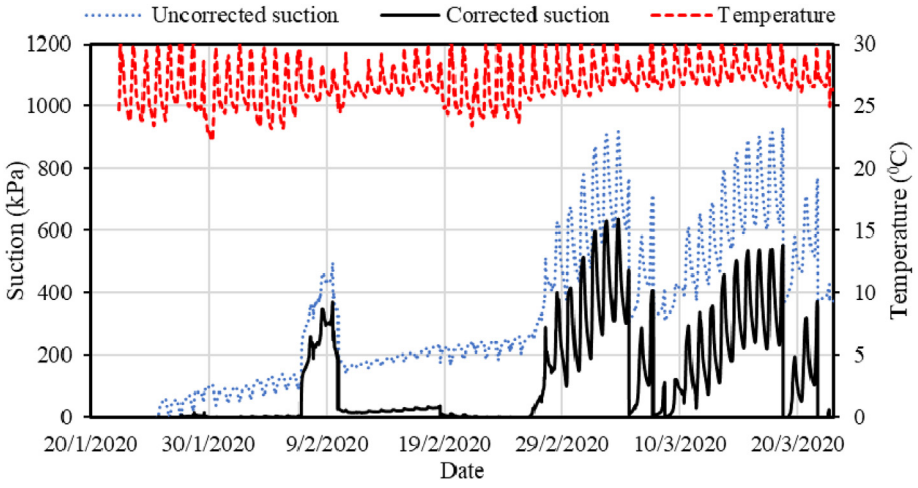

Fig. 11. Field monitoring of NTU Osmotic Tensiometer located at 0.15m depth.

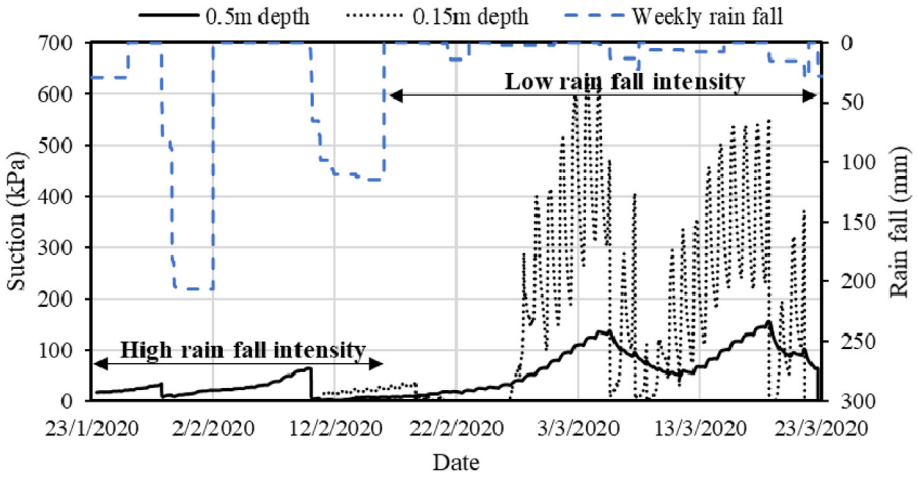

Fig. 12. Field monitoring of the two NTU Osmotic Tensiometer.

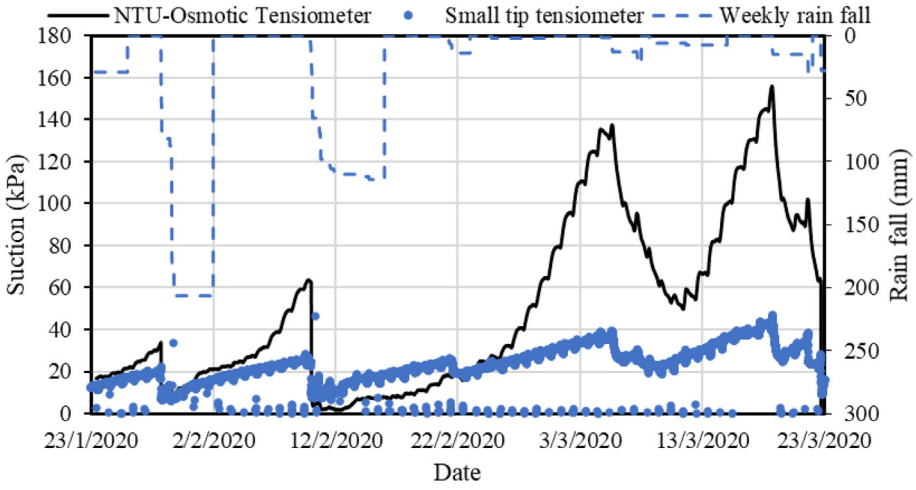

Fig. 13. Comparison between NTU Osmotic Tensiometer and small tip tensiometer at 0.5m depth.

especially in the lower suction range. However, as the small tip tensiometer capacity is between 60 and 100 kPa (Guan & Fredlund, 1997; Ridley and Burland, 1993), it is unable to respond well when the soil suction goes higher during the dry period. On the other hand, NTU Osmotic Tensiometer does not suffer the same limitation.

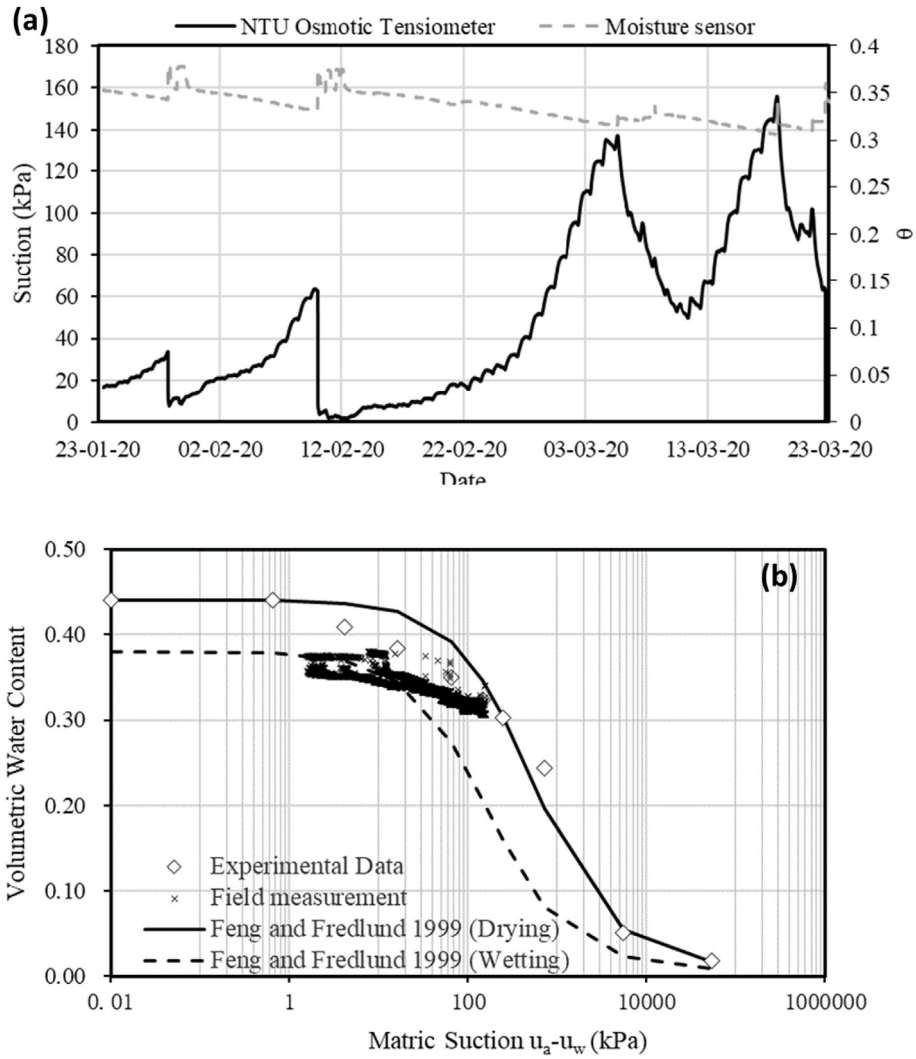

Fig. 14. (a) Suction and moisture content reading and (b) Field measurement on SWCC plot.

Table 2
Feng and Fredlund (1999) SWCC parameters.

Feng and Fredlund (1999)		
Parameters	Drying	Wetting
θ_u	0.441	0.380
B (kPa^d)	599	191
c	0.038	0.038
d	0.995	0.995
s_r (kPa)	540.130	531.207

Fig. 14(a) shows both volumetric water content reading from moisture sensor and suction measurement from NTU Osmotic Tensiometer while Fig. 14(b) shows the correlation between suction and volumetric water content from the field measurement in SWCC plot. Fig. 14(b) also shows the SWCC model developed using Feng and Fredlund (1999) SWCC hysteresis model with the SWCC parameters are shown in Table 2. The wetting parameters are obtained from the scaling method described in Pham et al. (2005).

The field measurements are located along the scanning curve which is reasonable as the soil on site has already been subjected to cycle of drying and wetting. While field measurement will not go into a very high suction range, the measured field data can be used to pinpoint the location of the scanning curve. The location of the scanning curve also indicates the past maximum suction that might have occurred in the slope. The location of the scanning curve might be the most relevant part of SWCC in conducting SWCC analysis as change in suction due to drying and wetting on the slope will occur in this line. The use of drying curve or wetting curve to estimate suction on a site is inaccurate as the suction-moisture content relationship of soil on site is located along the scanning curve. The field instrumentation appears to be a good and reliable method in obtaining the slope of the scanning curve.

4. Conclusions

Several conclusions can be derived from this study as follows:

(1) A new suction probe which is referred to as NTU Osmotic Tensiometer has been evaluated for real-time measurement of drying, wetting, and scanning curves of SWCC in the field.
(2) The readings from NTU Osmotic Tensiometer agreed well with the suction measurements from small tip tensiometers within the low suction range. However, NTU Osmotic Tensiometer is able to measure suction up to 600 kPa.
(3) NTU Osmotic Tensiometer has been proven to have high durability when subjected to drying and wetting cycles due to weather changes. A long-term measurement for a duration of 3 months demonstrated that there was no problem with NTU Osmotic Tensiometer during the measurement.
(4) The procedure and mathematical model for calibrations against temperature and pressure decay are proposed to enable accurate measurements using NTU Osmotic Tensiometer. Both the effect of temperature and pressure decay can be represented by a linear model.

Acknowledgments

This research was developed with the project “New Soil-Water Management Technologies for Sustainable Urban Greenery” supported by the National Parks Board Singapore, NEWRI, and Nanyang Technological University.

References

Bakker, G., van der Ploeg, M. J., de Rooij, G. H., Hoogendam, C. W., Gooren, H. P. A., Huiskes, C., Koopal, L. K., & Kruidhof, H. (2007). New polymer tensiometers: Measuring matric pressures down to the wilting point. *Vadose Zone Journal, 6*, 196–202.
Biesheuvel, P. M., & Verweij, H. (1999). Design of ceramic membrane supports permeability, tensile strength and stress. *Journal of Membrane Science, 156*(1), 141–152.
Bocking, K. A., & Fredlund, D. G. (1979). Use of the osmotic tensiometer to measure negative pore-water pressure. *Geotechnical Testing Journal, 2*(1), 3–10.
Chen, R., Liu, J., Li, J. H., & Ng, C. W. W. (2015). An integrated high-capacity tensiometer for measuring water retention curves continuously. *Soil Science Society of America Journal, 79*(3), 943–947. https://doi.org/10.2136/sssaj2014.11.0438n
Feng, M., & Fredlund, D. G. (1999). Hysteretic influence associated with thermal conductivity sensor measurements. Proceedings from theory to the practice of unsaturated soils mechanics in association with the 52nd Canadian geotechnical conference and the unsaturated soil group. *Regina, Sask, 14*, 14–20.
Fredlund, D. G., & Rahardjo, H. (1993). *Soil mechanics for unsaturated soils*. New York: Wiley, 1993.
Fredlund, D. G., Rahardjo, H., & Fredlund, M. D. (2012). *Unsaturated soil mechanics in Engineering practice*. New Jersey: John Wiley & Sons, Inc.
Fredlund, D. G., & Xing, A. (1994). Equations for the soil-water characteristic curve. *Canadian Geotechnical Journal, 31*(4), 521–532. https://doi.org/10.1139/t94-061
Guan, Y., & Fredlund, D. G. (1997). Use of the tensile strength of water for the direct measurement of high soil suction. *Canadian Geotechnical Journal, 34*(4), 604–614. https://doi.org/10.1139/t97-014
Haines, W. B. (1930). Studies in the physical properties of soil - V:The hysteresis effect in capillary properties and the modes of water distribution associated therewith. *Journal of Agricultural Science, 20*(1), 97–116.
Kristo, C., Rahardjo, H., & Satyanaga, A. (2017). Effect of variations in rainfall intensity on slope stability in Singapore. *International Soil and Water Conservation Research, 5*, 258–264. https://doi.org/10.1016/j.iswcr.2017.07.001
Kristo, K., Rahardjo, H., & Satyanaga, A. (2019). Effect of hysteresis on the stability of residual soil slope. *International Soil and Water Conservation Research, 7*(3), 226–238. https://doi.org/10.1016/j.iswcr.2019.05.003
Leong, E. C., & Rahardjo, H. (1997). Review of soil-water characteristic curve equations. *Journal of Geotechnical and Geoenvironmental Engineering, 123*(12), 1106–1117.
Liu, G., Toll, D., Kong, L., & Asquith, J. (2020). *Matric suction and volume characteristics of compacted clay soil under drying and wetting cycles*.
Lourenço, S. D. N., Gallipoli, D., Toll, D. G., Augarde, C. E., & Evans, F. D. (2011). A new procedure for the determination of soil-water retention curves by continuous drying using high-suction tensiometers. *Canadian Geotechnical Journal, 48*(2), 327–335. https://doi.org/10.1139/T10-062
Lourenço, S.D.N., Gallipoli, D., Toll, D.G., Evans, F.D., 2006. Development of a commercial tensiometer for triaxial testing of unsaturated soils, Unsaturated Soils 2006.
Peck, A. J., & Rabbidge, R. M. (1969). Design and performance of an osmotic tensiometer for measuring capillary potential. *Soil Science Society of America Journal, 33*, 196–202.
Pham, H. Q., Fredlund, D. G., & Barbour, S. L. (2005). A study of hysteresis models for soil-water characteristic curves. *Canadian Geotechnical Journal, 42*(6), 1548–1568.
Rahardjo, H., Kim, Y., & Satyanaga, A. (2019a). Role of unsaturated soil mechanics in geotechnical engineering. *International Journal of Geo-Engineering, 10*(1), 1–23.
Rahardjo, H., Satyanaga, A., Leong, E. C., Ng, Y. S., Foo, M. D., & Wang, C. L. (2007). Proceedings of 10th Australia New Zealand Conference on Geomechanics “Common Ground”. Brisbane, Australia, 21-24 October. *Slope failures in Singapore due to rainfall* (Vol. 2, pp. 704–709).
Rahardjo, H., Satyanaga, A., Mohamed, H., Ip, C. Y., & Rishi, S. S. (2019b). Comparison of soil-water characteristic curves from conventional testing and combination of small-scale centrifuge and dew point methods. *Journal of Geotechnical and Geological Engineering, 37*(2), 659–672.
Rahardjo, H. and Satyanaga, A. (2019), Sensing and monitoring for assessment of rainfall-induced slope failures in residual soil, Geotechnical Engineering. November 2019. Vol 172. Issue GE6. 10.1680/jgeen.18.00208.
Rahardjo, H., Shen, Y., Lee, D., Rivera, J. R., Nong, X., & Hamdany, A. H. (2020). New osmotic tensiometer development. *Geotechnical Testing Journal.* Accepted for publication in November 2020.
Ridley, A. M., & Burland, J. B. (1993). A New Instrument for the Measurement of Soil Moisture Suction. *Geotechnique, 43*, 321–324. https://doi.org/10.1680/geot.1993.43.2.321
Satyanaga, A., & Rahardjo, H. (2019). Unsaturated shear strength of soil with bimodal soil-water characteristic curve, 2019 *Geotechnique. September, 69*(9), 828–832.
Satyanaga, A., Rahardjo, H., & Hua, C. J. (2019). Numerical simulation of capillary barrier system under rainfall infiltration. August 2019 *ISSMGE International Journal of Geoengineering Case Histories, 5*(1), 43–54.
Satyanaga, A., Rahardjo, H., Leong, E.-C., & Wang, J.-Y. (2013). Water characteristic curve of soil with bimodal grain-size distribution, 0 *Computers and Geotechnics, 48*, 51–61. https://doi.org/10.1016/j.compgeo.2012.09.008.
Satyanaga, A., Zhai, Q., & Rahardjo, H. (2017). “Estimation of unimodal water characteristic curve for gap-graded soil”. October *Soils and Foundations, 57*(5),

789–801.
Satyanaga, A. and Rahardjo, H. (2020) Stability of Unsaturated Soil Slopes Covered with Melastoma Malabathricum in Singapore. Geotechnical Engineering. September 2020. Vol 7, No 6, pp. 393-403 10.1680/jenge.17.00031; ISSN 1353-2618 | E-ISSN 1751-8563.
Sun, D.-M., Li, X.-M., Feng, P., & Zang, Y.-G. (2016). Stability analysis of unsaturated soil slope during rainfall infiltration using coupled liquid-gas-solid three-phase model. *Water Science and Engineering, 9*(3), 183–194.
Sweeney, D. J. (1982). Some in situ soil suction measurements in Hong Kong's residual soil slopes. In *7th Southeast Asian Regional Conference.) Southeast Asian Geotechnical Society, Hong Kong* (Vol. 1, pp. 91–106).
Tami, D., Rahardjo, H., & Leong, E.-C. (2004). Effects of hysteresis on steady-state infiltration in unsaturated slopes. *Journal of Geotechnical and Geoenvironmental Engineering, 130*(9), 956–967. https://doi.org/10.1061/(ASCE)1090-0241(2004)130:9(956)
Toll, D. G., Lourenço, S. D. N., & Mendes, J. (2013). Advances in suction measurements using high suction tensiometers. *Engineering Geology, 165*, 29–37. https://doi.org/10.1016/j.enggeo.2012.04.013
Toll, D. G., Mendes, J., Gallipoli, D., Glendinning, S., & Hughes, P. N. (2012). Investigating the impacts of climate change on slopes: Field measurements. *Geological Society, London, Engineering Geology Special Publications, 26*(1), 151–161. https://doi.org/10.1144/egsp26.17
Wijaya, M., & Leong, E. C. (2016). Performance of high-capacity tensiometer in constant water content oedometer test. *International Journal of Geo-Engineering, 7*(1), 13. https://doi.org/10.1186/s40703-016-0027-6
Wijaya, M., Leong, E. C., & Rahardjo, H. (2014). CRS compression tests of an unsaturated kaolin with pore-water pressure measurement. In N. Khalili, A. R. Russell, & A. Khoshghalb (Eds.), *Unsaturated soils: Research & applications*. Australia: CRC Press Taylor & Francis.
Wijaya, M., Leong, E. C., & Rahardjo, H. (2015). Effect of shrinkage on air-entry value of soils. *Soils and Foundations, 55*(1), 166–180. https://doi.org/10.1016/j.sandf.2014.12.013
Zhai, Q., Rahardjo, H., & Satyanaga, A. (2017a). Uncertainty in the estimation of hysteresis of soil-water characteristic curve. *Environmental Geotechnics*. https://doi.org/10.1680/jenge.17.00008 (Published Online in November 2017).
Zhai, Q., Rahardjo, H., & Satyanaga, A. (2018). A pore-size distribution function based method for estimation of hydraulic properties of sandy soils. November *Engineering Geology, 246*, 288–292.
Zhai, Q., Rahardjo, H., Satyanaga, A., Dai, G., & Du, Y. J. (2020b). "Estimation of the wetting scanning curves for sandy soils" (Accepted in Apr 2020) *Engineering Geology, 272*, 105635. https://doi.org/10.1016/j.enggeo.2020.105635.
Zhai, Q., Rahardjo, H., Satyanaga, A., Dai, G., & Zhuang, Y. (2020a). "Framework to estimate the soil-water characteristic curve for soils with different void ratios". *Bulletin of Engineering Geology and the Environment, 79*(8), 1–11. https://doi.org/10.1007/s10064-020-01825-8 (Accepted in Apr 2020).
Zhai, Q., Rahardjo, H., Satyanaga, A., & Priono. (2017b). Effect of bimodal soil-water characteristic curve on the estimation of permeability function. *Engineering Geology, 230*, 142–151.
Zhai, Q., Rahardjo, H., Satyanaga, A., Priono, & Dai, G. (2019). Role of the pore-size distribution function on water flow in unsaturated soil. January *Journal of Zhejiang University - Science, 20*(1), 10–20.